



LAWRENCE
LIVERMORE
NATIONAL
LABORATORY

Reynolds-Averaged Navier-Stokes Modeling of Reshocked Richtmyer-Meshkov Instability Experiments and Simulations

J. T. Moran-Lopez, O. Schilling, J. P. Holloway

April 15, 2013

29th International Shock Wave Symposium
Madison, WI, United States
July 14, 2013 through July 19, 2013

Disclaimer

This document was prepared as an account of work sponsored by an agency of the United States government. Neither the United States government nor Lawrence Livermore National Security, LLC, nor any of their employees makes any warranty, expressed or implied, or assumes any legal liability or responsibility for the accuracy, completeness, or usefulness of any information, apparatus, product, or process disclosed, or represents that its use would not infringe privately owned rights. Reference herein to any specific commercial product, process, or service by trade name, trademark, manufacturer, or otherwise does not necessarily constitute or imply its endorsement, recommendation, or favoring by the United States government or Lawrence Livermore National Security, LLC. The views and opinions of authors expressed herein do not necessarily state or reflect those of the United States government or Lawrence Livermore National Security, LLC, and shall not be used for advertising or product endorsement purposes.

Reynolds-Averaged Navier–Stokes Modeling of Reshocked Richtmyer–Meshkov Instability Experiments and Simulations

J. Tiberius Morán-López¹, Oleg Schilling², and James P. Holloway¹

1 Introduction

Turbulence generated by hydrodynamic instabilities is important in high-energy-density physics [1]. Examples in astrophysics include turbulent mixing processes during stellar core-collapse, where shock waves accelerate multiple perturbed gas interfaces. Thermonuclear fuel compression in inertial confinement fusion is susceptible to shock-induced instabilities affecting the efficiency of target implosions and neutron yields [2]. Related applications include shock tube and high-energy laser experiments. Richtmyer–Meshkov instability is an important mechanism for the production of shock-induced turbulent mixing in these applications—the impulsive acceleration of a perturbed interface initially separating fluids with different densities results in the growth of perturbations and mixing. The interaction of the shock wave with the first fluid accelerates the interface and amplifies distortions on both the interface and shock [3, 4]. These perturbations result in the penetration of bubbles of light fluid into the heavy fluid and penetration of spikes of heavy fluid into the light fluid [5]. At sufficiently large Reynolds numbers, turbulent mixing occurs within the layer generated by this interpenetration. Reshock, in which the mixing layer is subjected to additional shock–interface interactions rather than a single interaction [6], also occurs in many applications. Reshocked Richtmyer–Meshkov instability is important to better understand and model accurately, as it is a central mechanism for turbulent mixing in diverse applications [7]. The further development and assessment of turbulence models validated against experimental and numerical simulation data are important areas of contemporary hydrodynamics and turbulence research.

¹University of Michigan, Department of Nuclear Engineering and Radiological Sciences, Ann Arbor, MI 48109 USA · ²Lawrence Livermore National Laboratory, Livermore, CA 94550 USA

2 Governing Equations and Initial Conditions

Unlike previous work [8, 9, 10] considering the Reynolds-averaged Euler equations, the present study uses the multicomponent Reynolds-averaged Navier–Stokes (RANS) equations coupled to a two-equation K – ε turbulence model accounting for heat conduction, viscous effects, and enthalpy diffusion [11, 12] to describe the transport of mean density $\bar{\rho}$, velocity \tilde{v}_i , total energy \tilde{e} , and heavy gas mass fraction \tilde{m}_H . The mean and turbulent transport equations are

$$\frac{\partial \bar{\rho}}{\partial t} + \frac{\partial}{\partial x_j} (\bar{\rho} \tilde{v}_j) = 0, \quad (1)$$

$$\frac{\partial}{\partial t} (\bar{\rho} \tilde{v}_i) + \frac{\partial}{\partial x_j} (\bar{\rho} \tilde{v}_i \tilde{v}_j) = -\frac{\partial \bar{p}}{\partial x_i} - \frac{\partial \tau_{ij}}{\partial x_j} + \frac{\partial \bar{\sigma}_{ij}}{\partial x_j}, \quad (2)$$

$$\begin{aligned} \frac{\partial}{\partial t} (\bar{\rho} \tilde{e}) + \frac{\partial}{\partial x_j} (\bar{\rho} \tilde{e} \tilde{v}_j) = & -\frac{\partial}{\partial x_j} (\bar{p} \tilde{v}_j) - \frac{\partial}{\partial x_j} (\bar{p} \tilde{v}_j') - \frac{\partial}{\partial x_j} (\tau_{ij} \tilde{v}_i) + \frac{\partial \bar{H}_j}{\partial x_j} \\ & + \frac{\partial}{\partial x_j} \left(\bar{\kappa} \frac{\partial \tilde{T}}{\partial x_j} + \frac{\mu_t}{\sigma_U} \frac{\partial \tilde{U}}{\partial x_j} \right) + \frac{\partial}{\partial x_j} \left[\left(\bar{\mu} + \frac{\mu_t}{\sigma_K} \right) \frac{\partial K}{\partial x_j} \right], \end{aligned} \quad (3)$$

$$\frac{\partial}{\partial t} (\bar{\rho} \tilde{m}_H) + \frac{\partial}{\partial x_j} (\bar{\rho} \tilde{m}_H \tilde{v}_j) = \frac{\partial}{\partial x_j} \left[\left(\bar{\rho} \bar{D} + \frac{\mu_t}{\sigma_m} \right) \frac{\partial \tilde{m}_H}{\partial x_j} \right], \quad (4)$$

$$\frac{\partial}{\partial t} (\bar{\rho} K) + \frac{\partial}{\partial x_j} (\bar{\rho} K \tilde{v}_j) = -\bar{v}_j' \frac{\partial \bar{p}}{\partial x_j} - \tau_{ij} \frac{\partial \tilde{v}_i}{\partial x_j} - \bar{\rho} \varepsilon + \frac{\partial}{\partial x_j} \left[\left(\bar{\mu} + \frac{\mu_t}{\sigma_K} \right) \frac{\partial K}{\partial x_j} \right], \quad (5)$$

$$\begin{aligned} \frac{\partial}{\partial t} (\bar{\rho} \varepsilon) + \frac{\partial}{\partial x_j} (\bar{\rho} \varepsilon \tilde{v}_j) = & -C_{\varepsilon 0} \frac{\varepsilon}{K} \bar{v}_j' \frac{\partial \bar{p}}{\partial x_j} - C_{\varepsilon 1} \frac{\varepsilon}{K} \tau_{ij}^d \frac{\partial \tilde{v}_i}{\partial x_j} - \frac{2}{3} C_{\varepsilon 3} \bar{\rho} \varepsilon \frac{\partial \tilde{v}_j}{\partial x_j} \\ & - C_{\varepsilon 2} \frac{\bar{\rho} \varepsilon^2}{K} + \frac{\partial}{\partial x_j} \left[\left(\bar{\mu} + \frac{\mu_t}{\sigma_\varepsilon} \right) \frac{\partial \varepsilon}{\partial x_j} \right], \end{aligned} \quad (6)$$

where overbars and tildes denote Reynolds and Favre averaged fields, respectively. The mean total energy includes the mean kinetic, mean internal, and turbulent kinetic energies, $\tilde{e} = \frac{\tilde{v}^2}{2} + \tilde{U} + K$. The molecular transport and thermodynamic coefficients are the mean dynamic viscosity $\bar{\mu}$, mass diffusivity \bar{D} , thermal conductivity $\bar{\kappa}$, and enthalpy diffusion \bar{H}_j . The closures for the Reynolds stress and averaged fluctuating velocity are $\tau_{ij} = \frac{2}{3} \bar{\rho} K \delta_{ij} - 2\mu_t \left(\tilde{S}_{ij} - \delta_{ij} \frac{\tilde{S}_k^k}{3} \right)$ and $\bar{v}_j' = \frac{v_t}{\sigma_\rho \bar{\rho}} \left(\frac{\partial \bar{p}}{\partial x_j} - \frac{\bar{p}}{\bar{\rho}} \frac{\partial \bar{p}}{\partial x_j} \right)$, respectively, where the turbulent viscosity is $v_t = \frac{\mu_t}{\bar{\rho}} = \frac{C_\mu K^2}{\varepsilon}$.

Defining the initial seed K_0 , Atwood number $At = (\rho_1 - \rho_2)/(\rho_1 + \rho_2)$, post-reshock velocity v_0 , and Richtmyer growth rate $\omega = (2\pi/\lambda_{rms}) |At| \Delta v$ with pertur-

bation wavelength λ_{rms} and shock-induced change in velocity Δv , the initial turbulent kinetic energy and dissipation rate are $K(x, 0) = K_0 (At v_0)^2$ and $\varepsilon(x, 0) = K(x, 0) \omega$, respectively. Using the heavy gas mole fraction [13] to define the spike and bubble locations $h_s(t)$ and $h_b(t)$ with 2%–98% mole fraction limits [11], the mixing layer width is $h(t) = h_s(t) - h_b(t)$. The RANS equations are solved using a third-order finite-difference weighted essentially nonoscillatory code [11, 12].

3 RANS Modeling of Reshocked Richtmyer–Meshkov Experiments and Large-Eddy Simulations

Previous RANS modeling of reshocked Richtmyer–Meshkov instability and mixing [11] considered experiments with $1.24 \leq Ma_s \leq 1.98$ and Atwood numbers $At = \pm 0.67$ [3, 4]. In addition to comparing the predicted mixing layer width to experimental data, the model sensitivity to variations in the principal coefficients and initial conditions, and convergence under grid refinement were also investigated. A coefficient set that provided overall good predictions of pre- and post-reshock widths was established. The model was subsequently applied to investigate the mixing layer widths when the time of reshock was adjusted experimentally [14] by changing the test section length $\delta = 8, 9.8, 13.1, 17.2, 19.9, \text{ and } 23.5 \text{ cm}$. Figure 1 illustrates results for the six cases comparing model predictions with experimental data. The table compares post-reshock growth rates, and reshock times are also included, demonstrating the delay in compression of the interface by increasing δ . The mean experimental and RANS growth rates are 2.4×10^3 and $2.5 \times 10^3 \text{ cm/s}$, respectively.

Reshocked Richtmyer–Meshkov instability with different Atwood numbers (both positive and negative) is also of interest. Relatively little experimental work has been conducted for cases aside from $At = \pm 0.67$. Therefore, the present RANS model is further extended to model a set of six different cases with $At = \pm 0.21, \pm 0.67$, and ± 0.87 corresponding to combinations of air with CO_2 , SF_6 , and H_2 , respectively, and for which LES data are available [15]. Constant $Ma_s = 1.50$ and $\delta = 62 \text{ cm}$ were used for the six cases. The $Ma_s = 1.50, At = 0.67$ case is very similar to that investigated experimentally [3], for which model predictions agreeing well with measurements were achieved [11]. Thus, the same initial conditions and model coefficients were used in the present simulations.

Figure 2 shows mixing layer widths for $At = \pm 0.21, \pm 0.67$, and ± 0.87 . Initial positive Atwood number configurations generally result in a reflected expansion wave after reshock that interacts with the interface [15], while reverse configurations typically result in a second reshock. Thus, times for reshock τ_r , arrival of the expansion wave τ_e , and second reshock τ_{r2} are given in addition to the growth rates \dot{h} following reshock. The turbulent mixing widths generally evolve differently, especially after reshock, due to differences in the gas densities. For $At = 0.21$ and 0.67 (air is the light gas in both cases), the early-time width shows a weak dependence on At . However, a significant difference in reshock times is observed as more time is required for the shock to reflect from the endwall and reshock the layer. A larger

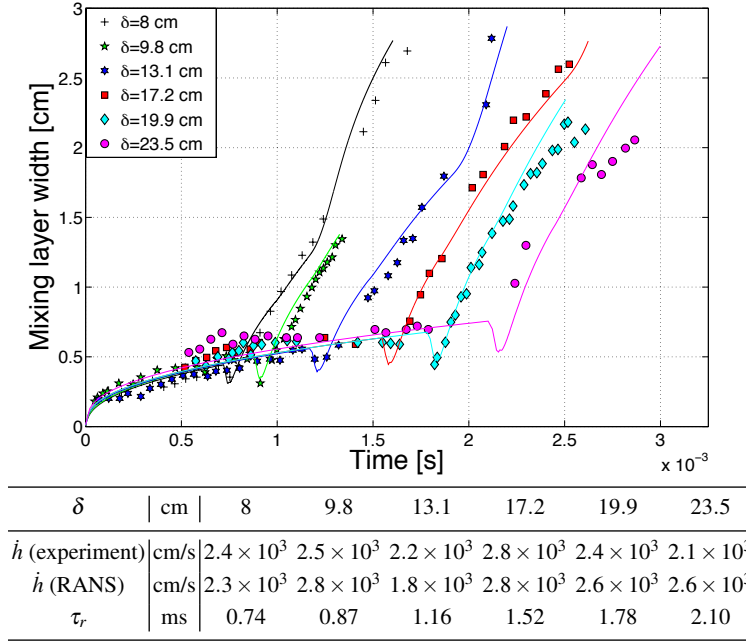


Fig. 1 Mixing layer widths, growth rates \dot{h} shortly after reshock, and reshock times τ_r for $\delta = 8, 9.8, 13.1, 17.2, 19.9, 23.5$ cm with $Ma_s = 1.20$, $At = 0.67$, $K_0 = 0.10$, $\lambda_{rms} = 0.25$ cm, $\sigma_p = 0.20$, and $C_{\epsilon 0} = 0.95$. The experimental data are from Ref. [14].

width is observed post-reshock for $At = 0.67$ due to a denser gas reshocking the interface. Reshock occurs earliest and mixing occurs at a higher rate after reshock for $At = 0.87$. Similar behavior is observed for the $At < 0$ cases. Although all of the gases in the driver section are different, similarities in initial mixing can be seen between $At = -0.87$ and -0.21 . The turbulent mixing layer widths also grow more rapidly as compared to the $At > 0$ cases.

4 Conclusions

A multicomponent RANS model coupled to a two-equation $K-\epsilon$ turbulence model was used to investigate reshocked Richtmyer–Meshkov instability for different reshock times by changing the test section length δ , as well as for different positive and negative Atwood numbers. The RANS model predictions were compared with experimental measurements [14] for the cases with different reshock times and with LES data [15] for the cases with different Atwood numbers. Decreasing δ resulted in earlier reshock times, while the post-reshock mixing layer growth rates changed relatively little, as observed in the experiments. The average experimental and RANS growth rates are $\dot{h} = 2.4 \times 10^3$ and $\dot{h} = 2.5 \times 10^3$ cm/s, respectively.

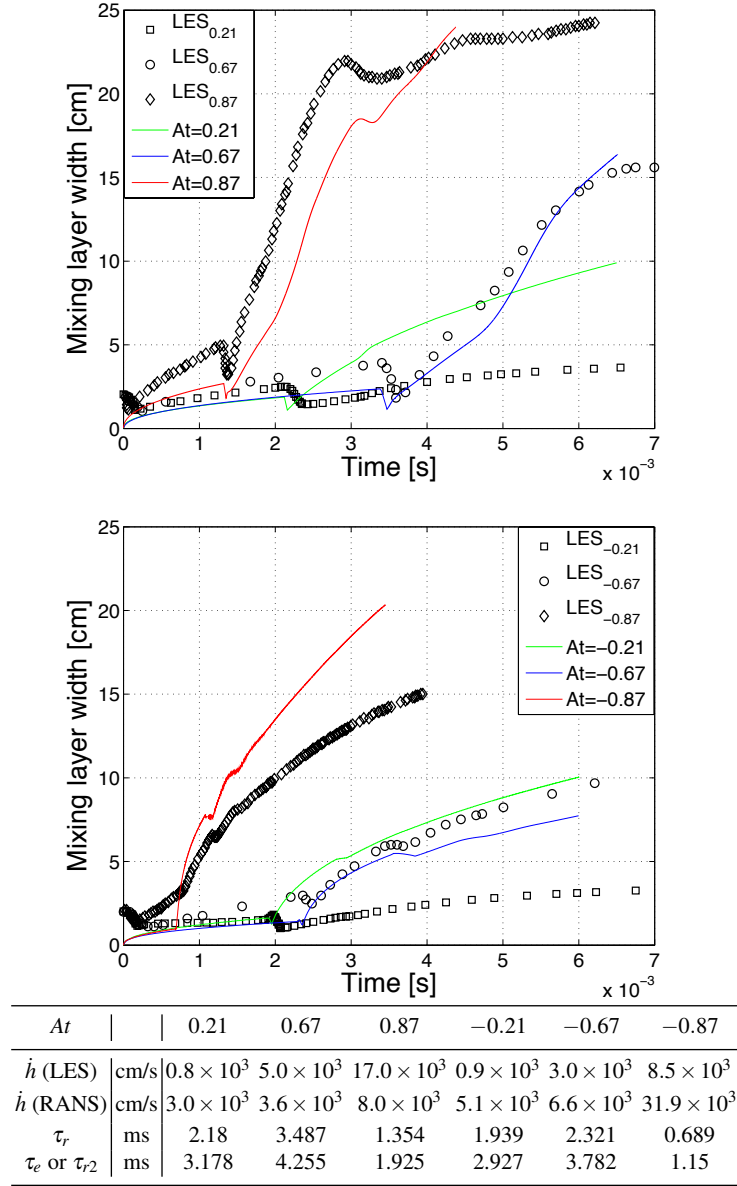


Fig. 2 Mixing layer widths, growth rates \dot{h} shortly after reshock, and reshock times τ_r for $At = \pm 0.21, \pm 0.67$, and ± 0.87 with $Ma_s = 1.50$, $\delta = 62$ cm, $K_0 = 0.10$, $\lambda_{rms} = 0.25$ cm, $\sigma_p = 0.90$, and $C_{\epsilon 0} = 0.90$. The LES data are from Ref. [15].

Larger growth rates also resulted from larger At values due to differences in the gas densities, while the post-reshock mixing layer widths for the $At < 0$ cases were larger than in the corresponding $At > 0$ cases.

Acknowledgments

This research was supported by the U.S. Department of Energy National Nuclear Security Administration under the Predictive Science Academic Alliances Program by grant DE-FC52-08NA28616 and performed under the auspices of the U.S. Department of Energy by Lawrence Livermore National Laboratory under contract number DE-AC52-07NA27344.

References

1. Zhou, Y., Remington, B.A., Robey, H.F., Cook, A.W., Glendinning, S.G., Dimits, A., Buckingham, A.C., Zimmerman, G.B., Burke, E.W., Peyser, T.A., Cabot, W., Eliason, D.: Progress in understanding turbulent mixing induced by Rayleigh-Taylor and Richtmyer-Meshkov instabilities. *Phys. Plasmas* **10**, 1883–1886 (2003)
2. Atzeni, S., Meyer-ter-Vehn, J.: *The Physics of Inertial Fusion: Beam Plasma Interaction, Hydrodynamics, Hot Dense Matter*, International Series of Monographs on Physics Vol. 125, Oxford University Press (2004)
3. Vetter, M., Sturtevant, B.: Experiments on the Richtmyer-Meshkov instability of an air/SF₆ interface. *Shock Waves* **4**, 247–252 (1995)
4. Poggi, F., Thoremby, M.-H., Rodriguez, G.: Velocity measurements in turbulent gaseous mixtures induced by Richtmyer-Meshkov instability. *Phys. Fluids* **10**, 2698–2700 (1998)
5. Brouillette, M.: The Richtmyer-Meshkov instability. *Annu. Rev. Fluid Mech.* **34**, 445–468 (2002)
6. Brouillette, M., Sturtevant, B.: Experiments on the Richtmyer-Meshkov instability: single-scale perturbations on a continuous interface. *J. Fluid Mech.* **263**, 271–292 (1994)
7. Schilling, O., Latini, M., Don, W.S.: Physics of reshock and mixing in single-mode Richtmyer-Meshkov instability. *Phys. Rev. E* **76**, 026319 (2007); Erratum, *Phys. Rev. E* **85**, 049904 (2012)
8. Gauthier, S., Bonnet, M.: A k - ϵ model for turbulent mixing in shock-tube flows induced by Rayleigh-Taylor instability. *Phys. Fluids A* **2**, 1685–1694 (1990)
9. Dimonte, G., Tipton, R.: K - L turbulence model for the self-similar growth of Rayleigh-Taylor and Richtmyer-Meshkov instabilities. *Phys. Fluids* **18**, 085101 (2006)
10. Banerjee, A., Gore, R.A., Andrews, M.J.: Development and validation of a turbulent-mix model for variable density and compressible flows. *Phys. Rev. E* **82**, 046309 (2010)
11. Morán-López, J.T., Schilling, O.: Multicomponent Reynolds-averaged Navier-Stokes simulations of reshocked Richtmyer-Meshkov instability-induced mixing. *High Energy Density Physics* **9**, 112–121 (2013)
12. Morán-López, J.T., Schilling, O.: Multicomponent Reynolds-averaged Navier-Stokes simulations of Richtmyer-Meshkov instability and mixing induced by reshock at different times. submitted (2013)
13. Latini, M., Schilling, O., Don, W.S.: Effects of WENO flux reconstruction order and spatial resolution on reshocked two-dimensional Richtmyer-Meshkov instability. *J. Comput. Phys.* **221**, 805–836 (2007)
14. Leinov, E., Malamud, G., Elbaz, Y., Levin, L.A., Ben-Dor, G., Shvarts, D., Sadot, O.: Experimental and numerical investigation of the Richtmyer-Meshkov instability under re-shock conditions. *J. Fluid Mech.* **626**, 449–475 (2009)
15. Lombardini, M., Hill, D.J., Pullin, D.I., Meiron, D.I.: Atwood ratio dependence of Richtmyer-Meshkov flows under reshock conditions using large-eddy simulations. *J. Fluid Mech.* **670**, 439–480 (2011)